Farquharson Louise (Orcid ID: 0000-0001-8884-511X)
Romanovsky Vladimir E. (Orcid ID: 0000-0002-9515-2087)
Cable William L (Orcid ID: 0000-0002-7951-3946)
Walker Donald A (Orcid ID: 0000-0001-9581-7811)
Nicolsky Dmitry J (Orcid ID: 0000-0001-9866-1285)

Climate change drives widespread and rapid thermokarst development in very cold permafrost in the Canadian High Arctic

[a] Louise M. Farquharson
[a] Vladimir E. Romanovsky
[b] William L. Cable
[c] Donald A. Walker
[d] Steven Kokelj
[a] Dimitry Nicolsky

[a]*Geophysical Institute Permafrost Laboratory, University of Alaska Fairbanks, Fairbanks, Alaska, USA*
[b]*Alfred Wegner Institute, Helmholtz Centre for Polar and Marine Research, Potsdam, Germany*
[c]*Institute of Arctic Biology, University of Alaska Fairbanks, Fairbanks, Alaska, USA*
[d]*Northwest Territories Geological Survey, Yellowknife, Northwest Territories Canada*

Key Points

- Observed thermokarst development in very cold permafrost at 3 monitoring sites along a 700 km transect in the Canadian High Arctic.
- Rapid landscape response to above average summer warmth is due to limited thermal buffering from overlying ecosystem components and near-surface ground ice.
- Change was greatest at Mould Bay where thawing index values were 240 % above historic normals causing ~90 cm of subsidence in 12 years.

This article has been accepted for publication and undergone full peer review but has not been through the copyediting, typesetting, pagination and proofreading process which may lead to differences between this version and the Version of Record. Please cite this article as doi: 10.1029/2019GL082187

Abstract

Climate warming in regions of ice-rich permafrost can result in widespread thermokarst development, which reconfigures the landscape and damages infrastructure. We present multi-site time-series observations which couple ground temperature measurements with thermokarst development in a region of very cold permafrost. In the Canadian High Arctic between 2003 and 2016, a series of anomalously warm summers caused mean thawing indices to be 150 – 240 % above the 1979-2000 normal resulting in up to 90 cm of subsidence over the 12-year observation period. Our data illustrate that despite low mean annual ground temperatures, very cold permafrost (<-10°C) with massive ground ice close to the surface is highly vulnerable to rapid permafrost degradation and thermokarst development. We suggest that this is due to little thermal buffering from soil organic layers and near surface vegetation, and the presence of near surface ground ice. Observed maximum thaw depths at our sites are already exceeding those projected to occur by 2090 under RCP 4.5.

Plain Language Summary

Permafrost is ground that remains at or below 0°C for two years or longer and it underlies much of the Arctic. Permafrost in Arctic lowland regions is frequently characterized by large volumes of ground ice which causes the ground surface to collapse when it melts. As the Arctic warms, ice-rich permafrost degradation is expected to be widespread. Our data illustrates that very cold permafrost, which has a mean annual ground temperature of -10°C or lower, is experiencing a rapid increase in active layer thickness at annual time scales. At three permafrost monitoring sites in the Canadian Arctic we have observed that warmer than average summer air temperatures have caused the active layer to deepen, near-surface ground ice to melt, and the overlying ground surface to subside, in some cases leading to the formation of small thaw ponds. Our results show that very cold permafrost terrain is responding rapidly to ongoing warming.

1. Introduction

Arctic permafrost is rapidly responding to climate change (Kokelj et al., 2017; Liljedahl et al., 2016; Romanovsky et al., 2017). Between 1990 and 2016, an increase of up to 4°C has been observed in terrestrial permafrost (Romanovsky et al., 2017) and this trend is expected to continue as Arctic mean annual air temperatures increase at a rate twice that of lower latitudes (IPCC, 2013). At many locations this warming has caused the initial thaw of near-surface permafrost and melting of near-surface ground ice, primarily ice wedge ice (Fraser et al., 2018; Kanevskiy et al., 2017; Liljedahl et al., 2016). Where ground ice is present, permafrost degradation can alter the geomorphological configuration of landscapes (Kanevskiy et al., 2017; Kokelj et al., 2017), in turn impacting sediment flux (Kokelj et al., 2013; Lamoureux and Lafrenière, 2009; Rudy et al., 2017), hydrology (Woo et al., 2008), nutrient and carbon cycling (Littlefair et al., 2017; Vonk et al., 2015), and overlying infrastructure (Raynolds et al., 2014). As such, documenting observations that illustrate how changes in air temperature are closely coupled to those below ground is critical in order to validate predictions about the rate, magnitude, and impacts of permafrost degradation in coming decades and centuries.

The majority of top-down permafrost degradation studies focus on the geomorphic response of ice-rich permafrost to warming through the application of field surveys (Kanevskiy et al., 2017; Kokelj et al., 2015; Lewkowicz, 2007; Ward Jones et al., 2019), remote sensing (Frost et al., 2018; Kokelj et al., 2017; Lewkowicz and Way, 2019; Raynolds et al., 2014) and susceptibility mapping (Rudy et al., 2013). In such studies, regional climate records are frequently utilized in lieu of direct, local, ground and air temperature measurements, to infer the cause of permafrost degradation. Consequently, there is a scarcity of well documented examples that combine measured ground temperature data and field observations illustrating climate-driven top-down permafrost degradation and thermokarst development. As such the projected extent of top-down degradation, both in terms of how much thaw at any given site and also to what spatial extent, remains poorly constrained in part due to a lack of field observations.

To date, the vulnerability of High-Arctic landscapes to climate change driven permafrost degradation has been illustrated primarily through its impact on hydrology (Lamoureux and Lafrenière, 2009; Lewis et al., 2012), hillslope processes (Lewkowicz, 2007; Lewkowicz and Way, 2019; Segal et al., 2016), and downstream impacts on sedimentology and geochemistry

(Rudy et al., 2017). Such permafrost related disturbance events have been attributed to a higher than normal summer air temperature (Biskaborn et al., 2019; Kokelj et al., 2017; Lewkowicz, 2007; Ward Jones et al., 2019). Despite these observations, the documented changes are not directly linked to, or directly supported by, in-situ time series data to link warm summer air temperatures, corresponding changes in active layer thickness, and terrain response. Filling this knowledge gap will greatly improve our understanding of, and ability to project, how pan-Arctic warming and subsequent permafrost degradation will impact infrastructure, hydrology, biogeochemistry and ecology.

This study combines time series measurements of local ground and air measurements spanning a decade of rapid change with observations of terrain subsidence in the High-Arctic. We use this unique data set to demonstrate that the combination of near-surface ground-ice, and limited to low thermal buffering from overlying soil organic layers and vegetation make extensive lowland areas across the High-Arctic extremely vulnerable to rapid, top-down degradation of ice-rich permafrost and associated subsidence driven terrain alteration. We combine time-series ground temperature measurements with field observations of rapid thermokarst development to: 1) link climate change with physical processes that are impacting vast areas of ice-rich polygonal Arctic terrain (Fraser et al., 2018; Liljedahl et al., 2016), and 2) document observations that link an increase in summer warmth with top down thaw, and rates and magnitude of thermokarst development.

2. Study site and methods

Permafrost monitoring sites were established along a south to north environmental gradient at Green Cabin on Banks Island 73°N, Mould Bay on Prince Patrick Island 77°N, and Isachsen on Ellef Ringnes Island 78°N (Fig. 1A). At each site permafrost temperature and active layer depths were monitored between 2003 and 2017. The locations were chosen as representative of regional vegetation and soil conditions as part of the North American Arctic Transect project (Walker et al., 2008). Soil grain size at Green Cabin is sandy silt while soil at Mould Bay and Isachsen is silty clay (Everett, 1968; Ping et al., 2008; Walker et al., 2008) (Table S1). Massive ice is present primarily in the form of ice-wedges in polygon networks, which are prevalent in the region adjacent to each study site (Figs. S1-S4) (French and Egginton, 1973; St-Onge and Gullentops, 2005). Subtle ice-wedge polygon patterning was evident in each region from aerial observations conducted between 2003-2006. Sediment present between ice wedges also contains excess ice in the form of ice lenses and pore-ice, reaching ca. 18 %, 67 %, and 68% in volume for Green Cabin, Mould Bay, and Isachsen, respectively

(Michaelson et al., 2008). At the start of our observations the land surface at each field site exhibited little to no topographic variability due to thermokarst processes.

Boreholes were located adjacent to ice-wedges to minimize disturbance. Ground temperature profiles, in the surface boreholes, were measured using 1.2 meter long, 28mm diameter probes consisting of 11 thermistors encapsulated in an epoxy filled clear PVC tube and a separate surface temperature sensor (Measurement Research Corporation, Gig Harbor, WA). The spacing of the thermistors within the MRC probes was 3, 9, 18, 24, 32, 40, 47, 55, 70, 85 and 106 cm below the ground surface at the time of installation. The actual depth of the thermistors was recalculated yearly as the vertical position of the probe changed due to frost jacking and ground settlement. A CR10-X data logger (Campbell Scientific, Logan, UT) at each site measured the sensors every five minutes. In the summer of 2010, a shallow borehole was drilled at each site and instrumented with temperature sensors (107-temperature probes, Campbell Scientific, Logan, UT) positioned 1.5, 2 and 3 meters below the ground surface. Depth between the ground surface and ice-wedge top was measured at the start of the observation period by digging soil pits at sites adjacent to our monitoring stations (Fig S1-S3). Air temperature measurements for thawing index (Ti) (the cumulative number of thawing degree-days above 0°Celsius per year) calculations were collected using thermistor temperature sensors (107-temperature probe, Campbell Scientific, Logan, UT). Thawing index normals were calculated for 1979 – 2000 from historic climate records obtained from weather stations at Sachs Harbor, Isachsen, and Mould Bay (http://climate.weather.gc.ca/historical_data). The extent of thermokarst development was determined from repeat field surveys, oblique ground photographs, and structure from motion (SfM) derived digital elevation models (DEMs).

Observed maximum thaw depths (MTD) were compared to those derived from the Stefan equation, a simple analytical solution of heat transfer used to model active layer thickness:

$$MTD = \sqrt{\frac{2k_t \cdot TI * 86400}{\partial \cdot L}} \qquad (1)$$

Where k_t is the thawed thermal conductivity, TI is the thawing index value at the ground surface, ∂ is the volumetric ice content prior to thaw, L is the latent heat constant, and 86400 is the multiplier necessary to convert degree-days into degree-seconds to keep all units in the System International (SI).

The equation (eq. 1) has been used in the form

$MTD = A\sqrt{TI}$ (2), where $A = \sqrt{\frac{2k_t \cdot * 86400}{\partial \cdot L}}$

Because k_t and ∂ may vary from year to year due to changes in precipitation and soil moisture content, the coefficient A may not stay constant from year to year. We estimated the average value of A for each site by plotting the square root of the observed TI (°C-days) at each site and calculating the coefficient for the line of best fit. This allowed us to substitute $2k_t$, ∂, and L, for A and to use the equation (eq. 2) to calculate expected maximum thaw depths according to existing basic heat transfer physics.

To model the impact of increasing air temperature on the maximum thaw depth at each of our sites over coming decades we combined field observations of maximum thaw depth and TI (°C-days) with the 50th percentile of the multi-model ensemble for climate projections from the Coupled Model Intercomparison Project Phase 5 global climate model (CMIP5 GCM) (https://climate-change.canada.ca/climate-data/#/cmip5-data). To identify discrepancies between observed and modelled air temperature at each site, we compared ten years of field observations with GCM values between 2003 – 2016 and calibrated the model according to the offsets observed. The seasonal variations were adjusted by about 10% to match the observed air temperature. We combined calibrated GCM air temperature projections with coefficients (A) obtained from equation (eq. 2) to calculate mean decadal future TI (°C-day) values for 2020 - 2090 under representative concentration pathways (RCPs) 4.5 (moderate warming scenario) and 8.5 (extreme warming scenario) (IPCC, 2013) and to project active layer thickness (or "maximum thaw depth").

3. Results and discussion

3.1 Widespread and rapid thermokarst development driven by above normal summer air temperatures

We observed permafrost degradation and thermokarst development in the form of top down melt of ice-wedge ice across all three study sites during the period 2003-2016 (Fig. 1B, C). Active layer deepening and resultant thermokarst development occurred during summers with TI values higher than historical norms (Fig. 2A, Table S3) most notably during 2007, 2011 and 2012, when the thaw front intersected massive ice remarkably early in the season (Fig. 3). Mean TI values were 154 %, 239 % and 192 % of the historic normal (1979-2000) for GC, MB and IS respectively (Fig. 2A, for years used to calculate mean see Table S3). Thaw onset (illustrated in Fig. 4) began between late May and late June (on average starting on

June 7th, June 11th and June 14th for GC, MB, and IS, respectively). The thawing front intersected ice wedge tops (Figs. S1-3), on average, 50, 38, and 41 days after thaw onset and continued on average for 60, 44, and 31 days for GC, MB, and IS, respectively (Table S4). Adjacent to ice wedges, average maximum thaw depth was 85 cm, 54 cm, and 48 cm for GC, MB, and IS, respectively. Upwards freeze back of mineral soil adjacent to the ice wedges began shortly after the maximum thaw depth was reached and was earliest at IS (on average August 12th) and the latest at GC (on average August 27th). These average dates of mineral soil freeze back can be used as a good estimate for when ice melt stopped (Wainwright et al., 2015). Our data show that complete refreezing of the active layer took place on average by October 3rd, September 25th, and September 17th, for GC, MB, and IS, respectively (Table S4).

Deepening of the thaw front and subsequent ground-ice melt lead to surface subsidence, which was seen most acutely in the form of ice-wedge polygon trough deepening (Fig. 1B, C, Fig S4). The melting of ice-wedges resulted in up to 60 cm, 90 cm, and 40 cm of subsidence at GC, MB, and IS, respectively over the observation period (Figs. 1B, C, S4). Differential settlement occurred due to variation in ground ice content across ice-wedge polygons, with the greatest change in surface elevation occurring over ice wedges. As such, observed subsidence values for IS and MB should be considered as minimum values because the perennially frozen mineral soil in polygon centers contain between 18 % (GC) and 68 % (IS) of ice by volume (Michaelson et al., 2008) and may have also been subjected to subsidence upon thawing.

While patterns of topographic change were similar across all sites, the impact on hydrology varied. At GC no ponding occurred, possibly due to coarser grained soil facilitating the drainage of melt water (Fig. 1B, C). In contrast at MB and IS finer grain soils impeded drainage and resulted in the formation of shallow ponds with standing water up to 40 cm deep (Fig. 1B, C).

3.2 Key drivers of rapid top-down thaw of very cold permafrost

From our results, we identify three key factors which are responsible for widespread thaw at each of our study sites: an increase in summer warmth, limited thermal buffering from overlying soil organic layers and vegetation, and near surface massive ice.

Increased summer warmth: The rapid transfer of heat from air to soil in High-Arctic environments has been observed previously where short-lived but intense warm events are

thought to have forced widespread active layer deepening during a single warm summer of deeper thaw (Fraser et al., 2018; Lamoureux and Lafrenière, 2009; Lewis et al., 2012; Lewkowicz, 2007). Recent observations from the Canadian High-Arctic link higher than normal summer warmth to a rapid increase in thaw related processes including active layer detachment slide, retrogressive thaw slumps, and ice wedge melt (Fraser et al., 2018; Lewkowicz and Way, 2019; Ward Jones et al., 2019). Across all of our sites TI values were 2x to 3x higher than historical norms (1979 – 2000) throughout our observation period (2003 – 2016) (Fig. 2A, Table S3), and as established through basic analytical solutions for heat transfer such as the Stefan equation (eq. 1), there was a strong relationship between TI and active layer thickness (Nelson et al., 1997; Romanovsky and Osterkamp, 1997) (Fig. 2A). Interestingly, at IS, higher TI did not consistently produce the greatest thaw depths which suggests that other factors, such as ground ice content, interannual variations in soil moisture, and hours of direct sunlight (Lewkowicz, 2007) also play an important role in maximum thaw depth.

Sparse vegetation cover and no organic horizon of thermal significance: The presence of plant organic matter exerts an important control over how permafrost responds to climate warming. The accumulation of both living and dead vegetation can act as an important buffer for permafrost against changing air temperatures (Baughman et al., 2015; Raynolds et al., 2008; Shur and Jorgenson, 2007; Yi et al., 2007). All of our sites were characterized by limited to low thermal buffering from overlying ecosystem components due to the sparse vegetation cover in the form of graminoid tundra and cryptogamic crusts (Walker et al., 2005) (Table S2). While these vegetation classes act to provide a limited buffer for the underlying permafrost from warm summer air temperatures, their buffering effects are much less than those afforded by the thick moss and peat units which mantle much of the permafrost affected landscapes of the Low-Arctic (Baughman et al., 2015; Walker et al., 2005). Consequently, the gain and loss of heat in summer and winter respectively is more rapid at sites characterized by limited soil organic accumulation and vegetation (Fraser et al., 2018).

Near surface ground ice: At all of our sites, massive ground ice was present at the base of the active layer (Figs. S1-3) due to the permafrost being, until recently, in equilibrium with the climate. This facilitated a rapid geomorphological response to active layer deepening. During the summer months, once the depth of thaw exceeded the overlying protective sediment layer, continuous ice melt could occur and the extent of subsidence was limited primarily by

the duration of the thaw season (Fig. 4). For example, between 2005 and 2016 at IS, the active layer increased by ca. 0.2 m but the cumulative subsidence reached 0.4 m.

3.3 Comparing observed and modelled maximum thaw depth

As expected, our observations align fairly well with modelled MTD values derived from the Stefan equation (eq. 1) (Fig. 2B). However, we observed interannual variability that highlights the limitations of this model. The difference between observed and modelled values in any given year is due to the interannual variability of soil properties, namely the thawed thermal conductivity due to moisture content, and latent heat effects due to variations in the volume of any ice present prior to thaw. Interannual variations in soil moisture content occur in part due to the timing and volume of late summer and fall precipitation events, which can vary greatly from year to year. Modelled maximum thaw depth values fit best with our observations at Mould Bay and Green Cabin. In contrast, the difference between modelled and observed thaw depths vary more at Isachsen, possibly due to higher interannual variability in soil moisture and ice content in the active layer. Multivariate regression analysis showed that maximum winter snow depth had limited influence over maximum thaw depth when compared to the TI (°C-days) (Table S5). It is also important to note that due to the mechanisms described in Figure 4, simple analytical solutions such as the Stefan equation fail to capture the total depth of ice melt and associated subsidence, as cumulative subsidence can far exceed any increase in active layer depth even during a single summer.

3.4 Future change in a warmer High-Arctic

The rapid top down thaw process that we have documented across our three High-Arctic sites is likely to continue in coming decades to centuries. We combined our field observations and climate projections from the Coupled Model Intercomparison Project Phase 5 global climate model (CMIP5 GCM) (https://climate-change.canada.ca/climate-data/#/cmip5-data) to explore future thaw depths under IPCC RCP 4.5 and 8.5. Maximum thaw depths by 2090 were projected to be 108 cm and 129 cm at Green Cabin for RCP 4.5 and 8.5 respectively; 58 cm and 72 cm at Mould Bay for RCP 4.5 and 8.5 respectively; and 59 cm and 73 cm at Isachsen for RCP 4.5 and 8.5 respectively. For all sites, the maximum observed thaw depths observed since 2003 met or exceeded the projected thaw depths for 2090 under RCP 4.5, indicating that the depth of thaw is already routinely exceeding the thaw expected under temperatures projections from this scenario (Figure 2).

4. Conclusions

In this study we couple continuous time-series measurements of warming air and ground temperature with top-down permafrost thaw, ice-wedge melt, and formation of thermokarst terrain. We observe that High-Arctic landscapes respond rapidly to warmer summer temperatures and we demonstrate that in regions where ground ice was, until recently in equilibrium with climate, even a small increase in active layer depth is sufficient to cause ground subsidence totaling tens of centimeters. We find that limited thermal protection from soil organic layers and vegetation facilitates a rapid response to air warming. Our observations provide field-based evidence to explain observations reported by recent remote-sensing based investigations (Fraser et al., 2018; Liljedahl et al., 2016) and highlight the limitations of modelling active layer depth and near surface ice melt without ground truthing in the from field observations. We find that observed maximum thaw depths at all sites are already regularly exceeding modelled future thaw depths for 2090 under IPCC RCP 4.5. Our data show that very cold permafrost (<-10°C) at high latitudes is highly vulnerable to rapid near-surface permafrost degradation due to climate change.

Acknowledgements

LMF, VR, WC were funded by PermAON2, NSF grant number ARC-1107524. We thank Matthew Balazs and Richard Buzard for advice on structure-from-motion data collection. We thank Martha "Tako" Raynolds and two anonymous reviewers for helpful comments which greatly improved this manuscript. This manuscript benefitted from discussions with Daniel Mann, Guido Grosse, Yuri Shur, and Misha Kanevskiy. We thank our pilots from Ken Borek Air for transporting us safely to our remote field sites. Data from this paper is available from the real-time data portal at http://permafrost.gi.alaska.edu/.

References

Baughman, C.A., Mann, D.H., Verbyla, D.L., Kunz, M.L., 2015. Soil-surface organic layers in Arctic Alaska: Spatial distribution, rates of formation, microclimatic effects. J. Geophys. Res. G Biogeosciences 120, 1150–1164. https://doi.org/10.1002/2015JG002983

Biskaborn, B.K., Smith, S.L., Noetzli, J., Matthes, H., Vieira, G., Streletskiy, D.A., Schoeneich, P., Romanovsky, V.E., Lewkowicz, A.G., Abramov, A., Allard, M., Boike, J., Cable, W.L., Christiansen, H.H., Delaloye, R., Diekmann, B., Drozdov, D., Etzelmüller, B., Grosse, G., Guglielmin, M., Ingeman-Nielsen, T., Isaksen, K., Ishikawa, M., Johansson, M., Johannsson, H., Joo, A., Kaverin, D., Kholodov, A., Konstantinov,

P., Kröger, T., Lambiel, C., Lanckman, J.P., Luo, D., Malkova, G., Meiklejohn, I., Moskalenko, N., Oliva, M., Phillips, M., Ramos, M., Sannel, A.B.K., Sergeev, D., Seybold, C., Skryabin, P., Vasiliev, A., Wu, Q., Yoshikawa, K., Zheleznyak, M., Lantuit, H., 2019. Permafrost is warming at a global scale. Nat. Commun. https://doi.org/10.1038/s41467-018-08240-4

Everett, K.R., 1968. Soil development in the Mould Bay and Isachsen areas, Queen Elizabeth Islands, Northwest Territories, Canada. Research Foundation and the Institute of Polar Studies, The Ohio State University.

Fraser, R.H., Kokelj, S. V, Lantz, T.C., McFarlane-Winchester, M., Olthof, I., Lacelle, D., 2018. Climate Sensitivity of High Arctic Permafrost Terrain Demonstrated by Widespread Ice-Wedge Thermokarst on Banks Island. Remote Sens. 10.

French, H.M., Egginton, P., 1973. Thermokarst development, Banks Island, western Canadian Arctic, in: 2nd International Conference on Permafrost. pp. 203–212.

Frost, G., Christopherson, T., Jorgenson, M., Liljedahl, A., Macander, M., Walker, D., Wells, A., Frost, G. V., Christopherson, T., Jorgenson, M.T., Liljedahl, A.K., Macander, M.J., Walker, D.A., Wells, A.F., 2018. Regional Patterns and Asynchronous Onset of Ice-Wedge Degradation since the Mid-20th Century in Arctic Alaska. Remote Sens. https://doi.org/10.3390/rs10081312

IPCC, 2013. Summary for Policymakers, in: Climate Change 2013: The Physical Science Basis. Contribution of Working Group I to the Fifth Assessment Report of the Intergovernmental Panel on Climate Change. p. 33. https://doi.org/10.1017/CBO9781107415324

Kanevskiy, M., Shur, Y., Jorgenson, T., Brown, D.R.N., Moskalenko, N., Brown, J., Walker, D.A., Raynolds, M.K., Buchhorn, M., 2017. Degradation and stabilization of ice wedges: Implications for assessing risk of thermokarst in northern Alaska. Geomorphology 297, 20–42. https://doi.org/10.1016/j.geomorph.2017.09.001

Kokelj, S. V., Lacelle, D., Lantz, T.C., Tunnicliffe, J., Malone, L., Clark, I.D., Chin, K.S., 2013. Thawing of massive ground ice in mega slumps drives increases in stream sediment and solute flux across a range of watershed scales. J. Geophys. Res. Earth Surf. https://doi.org/10.1002/jgrf.20063

Kokelj, S. V., Lantz, T.C., Tunnicliffe, J., Segal, R., Lacelle, D., 2017. Climate-driven thaw of permafrost preserved glacial landscapes, northwestern Canada. Geology 45, 371–374. https://doi.org/10.1130/G38626.1

Kokelj, S. V., Tunnicliffe, J., Lacelle, D., Lantz, T.C., Chin, K.S., Fraser, R., 2015. Increased precipitation drives mega slump development and destabilization of ice-rich permafrost terrain, northwestern Canada. Glob. Planet. Change. https://doi.org/10.1016/j.gloplacha.2015.02.008

Lamoureux, S.F., Lafrenière, M.J., 2009. Fluvial impact of extensive active layer detachments, Cape Bounty, Melville Island, Canada. Arctic, Antarct. Alp. Res. 41, 59–68. https://doi.org/10.1657/1523-0430-41.1.59

Lewis, T., Lafrenière, M.J., Lamoureux, S.F., 2012. Hydrochemical and sedimentary responses of paired High Arctic watersheds to unusual climate and permafrost disturbance, Cape Bounty, Melville Island, Canada. Hydrol. Process. 26, 2003–2018. https://doi.org/10.1002/hyp.8335

Lewkowicz, A.G., 2007. Dynamics of Active-layer Detachment Failures , Fosheim Peninsula , Ellesmere Island , Nunavut , Canada. Permafr. Periglac. Process. 103, 89–103. https://doi.org/10.1002/ppp.578

Lewkowicz, A.G., Way, R.G., 2019. Extremes of summer climate trigger thousands of thermokarst landslides in a High Arctic environment. Nat. Commun. 10, 1329.

Liljedahl, A.K., Boike, J., Daanen, R.P., Fedorov, A.N., Frost, G. V, Grosse, G., Hinzman, L.D., Iijma, Y., Jorgenson, J.C., Matveyeva, N., Necsoiu, M., Raynolds, M.K., Romanovsky, V.E., Schulla, J., Tape, K.D., Walker, D.A., Wilson, C.J., Yabuki, H., Zona, D., 2016. Pan-Arctic ice-wedge degradation in warming permafrost and its influence on tundra hydrology. Nat. Geosci.

Littlefair, C.A., Tank, S.E., Kokelj, S. V., 2017. Retrogressive thaw slumps temper dissolved organic carbon delivery to streams of the Peel Plateau, NWT, Canada. Biogeosciences. https://doi.org/10.5194/bg-14-5487-2017

Michaelson, G.J., Ping, C.L., Epstein, H., Kimble, J.M., Walker, D.A., 2008. Soils and frost boil ecosystems across the North American Arctic Transect. J. Geophys. Res. Biogeosciences. https://doi.org/10.1029/2007JG000672

Nelson, F.E., Shiklomanov, N.I., Mueller, G.R., Hinkel, K.M., Walker, D.A., Bockheim, J.G., 1997. Estimating Active-Layer Thickness over a Large Region: Kuparuk River Basin, Alaska, U.S.A. Arct. Alp. Res. 29, 367. https://doi.org/10.2307/1551985

Ping, C.L., Michaelson, G.J., Kimble, J.M., Romanovsky, V.E., Shur, Y.L., Swanson, D.K., Walker, D.A., 2008. Cryogenesis and soil formation along a bioclimate gradient in Arctic North America. J. Geophys. Res. Biogeosciences. https://doi.org/10.1029/2008JG000744

Raynolds, M.K., Walker, D. a., Ambrosius, K.J., Brown, J., Everett, K.R., Kanevskiy, M., Kofinas, G.P., Romanovsky, V.E., Shur, Y., Webber, P.J., 2014. Cumulative geoecological effects of 62 years of infrastructure and climate change in ice-rich permafrost landscapes, Prudhoe Bay Oilfield, Alaska. Glob. Chang. Biol. 20, 1211–1224. https://doi.org/10.1111/gcb.12500

Raynolds, M.K., Walker, D.A., Munger, C.A., Vonlanthen, C.M., Kade, A.N., 2008. A map analysis of patterned-ground along a North American Arctic transect. J. Geophys. Res. Biogeosciences. https://doi.org/10.1029/2007JG000512

Romanovsky, V.E., Osterkamp, T.E., 1997. Thawing of the Active Layer on the Coastal Plain of the Alaskan Arctic. Permafr. Periglac. Process. https://doi.org/10.1002/(SICI)1099-1530(199701)8:1<1::AID-PPP243>3.3.CO;2-L

Romanovsky, V.E., Smith, S.L., Shiklomanov, N.I., Streletskiy, D.A., Isaksen, K., Kholodov, A.L., Christiansen, H.H., Drozdov, D.S., Malkova, G. V., Marchenko., S.S., 2017. Terrestrial permafrost, in: Blunden, J., Arndt, D.. (Eds.), State of the Climate in 2016. Bulletin of the American Meteorological Society. p. pp.ES1-ES32.

Rudy, A.C.A., Lamoureux, S.F., Kokelj, S. V., Smith, I.R., England, J.H., 2017. Accelerating Thermokarst Transforms Ice-Cored Terrain Triggering a Downstream Cascade to the Ocean. Geophys. Res. Lett. 44, 11,080-11,087. https://doi.org/10.1002/2017GL074912

Rudy, A.C.A., Lamoureux, S.F., Treitz, P., Collingwood, A., 2013. Identifying permafrost slope disturbance using multi-temporal optical satellite images and change detection techniques. Cold Reg. Sci. Technol. 88, 37–49. https://doi.org/10.1016/j.coldregions.2012.12.008

Segal, R.A., Lantz, T.C., Kokelj, S. V., 2016. Acceleration of thaw slump activity in

glaciated landscapes of the Western Canadian Arctic. Environ. Res. Lett. https://doi.org/10.1088/1748-9326/11/3/034025

Shur, Y.L., Jorgenson, M.T., 2007. Patterns of Permafrost Formation and Degradation in Relation to Climate and Ecosystems. Permafr. Periglac. Process. 18, 7–19. https://doi.org/10.1002/ppp.582

St-Onge, D., Gullentops, F., 2005. Morphodynamics of cold high latitude semiarid regions: The example of Ellef Ringnes Island, Nunavut. Géographie Phys. Quat. 59, 103–111.

Vonk, J.E., Tank, S.E., Bowden, W.B., Laurion, I., Vincent, W.F., Alekseychik, P., Amyot, M., Billet, M.F., Canário, J., Cory, R.M., Deshpande, B.N., Helbig, M., Jammet, M., Karlsson, J., Larouche, J., MacMillan, G., Rautio, M., Walter Anthony, K.M., Wickland, K.P., 2015. Reviews and Syntheses: Effects of permafrost thaw on arctic aquatic ecosystems. Biogeosciences Discuss. https://doi.org/10.5194/bgd-12-10719-2015

Wainwright, H.M., Dafflon, B., Smith, L.J., Hahn, M.S., Curtis, J.B., Wu, Y., Ulrich, C., Peterson, J.E., Torn, M.S., Hubbard, S.S., 2015. Identifying multiscale zonation and assessing the relative importance of polygon geomorphology on carbon fluxes in an Arctic tundra ecosystem. J. Geophys. Res. Biogeosciences. https://doi.org/10.1002/2014JG002799

Walker, D.A., Epstein, H.E., Romanovsky, V.E., Ping, C.L., Michaelson, G.J., Daanen, R.P., Shur, Y., Peterson, R.A., Krantz, W.B., Raynolds, M.K., Gould, W.A., Gonzalez, G., Nicolsky, D.J., Vonlanthen, C.M., Kade, A.N., Kuss, P., Kelley, A.M., Munger, C.A., Tarnocai, C.T., Matveyeva, N. V., Daniëls, F.J.A., 2008. Arctic patterned- ground ecosystems: A synthesis of field studies and models along a North American Arctic Transect. J. Geophys. Res. Biogeosciences 113. https://doi.org/10.1029/2007JG000504

Walker, D.A., Reynolds, M.K., Daniëls, F.J.A., Einarsson, E., Elvebakk, A., Gould, W.A., Katenin, A.E., Kholod, S.S., Markon, C.J., Melnikov, E.S., Moskalenko, N.G., Talbot, S.S., Yurtsev, B.A., Bliss, L.C., Edlund, S.A., Zoltai, S.C., Wilhelm, M., Bay, C., Gudjónsson, G., Moskalenko, N.G., Ananjeva, G. V., Drozdov, D.S., Konchenko, L.A., Korostelev, Y. V., Melnikov, E.S., Ponomareva, O.E., Matveyeva, N. V., Safranova, I.N., Shelkunova, R., Polezhaev, A.N., Johansen, B.E., Maier, H.A., Murray, D.F., Fleming, M.D., Trahan, N.G., Charron, T.M., Lauritzen, S.M., Vairin, B.A., 2005. The Circumpolar Arctic vegetation map. J. Veg. Sci. 16, 267–282.

https://doi.org/10.1111/j.1654-1103.2005.tb02365.x

Ward Jones, M.K., Pollard, W.H., Jones, B.M., 2019. Rapid initialization of retrogressive thaw slumps in the Canadian high Arctic and their response to climate and terrain factors. Environ. Res. Lett.

Woo, M.K., Kane, D.L., Carey, S.K., Yang, D., 2008. Progress in permafrost hydrology in the new millennium. Permafr. Periglac. Process. https://doi.org/10.1002/ppp.613

Yi, S., Woo, M.K., Arain, M.A., 2007. Impacts of peat and vegetation on permafrost degradation under climate warming. Geophys. Res. Lett. 34. https://doi.org/10.1029/2007GL030550

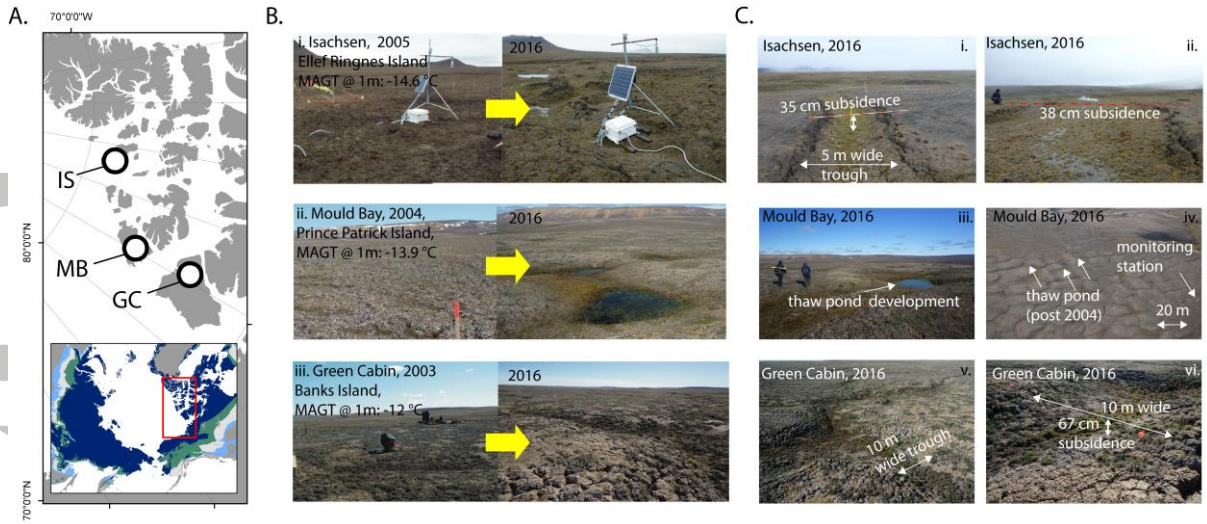

Figure 1. A. Map of the study area showing permafrost monitoring site locations. B. Examples of the even terrain at each site at the start of monitoring (2003, 2004, 2005) and the terrain after a decade of monitoring (2016). Thermokarst development was observed at all sites. C. Examples of thermokarst topography and landforms observed at each site in 2016: i), ii) subsidence and trough formation at Isachsen, iii) trough formation and pond development at Mould Bay, iv) subsidence and trough formation at Green Cabin. All images are taken from within 500 m of the permafrost monitoring station with the exception of *iv* which was taken aerially but includes the monitoring station within the frame.

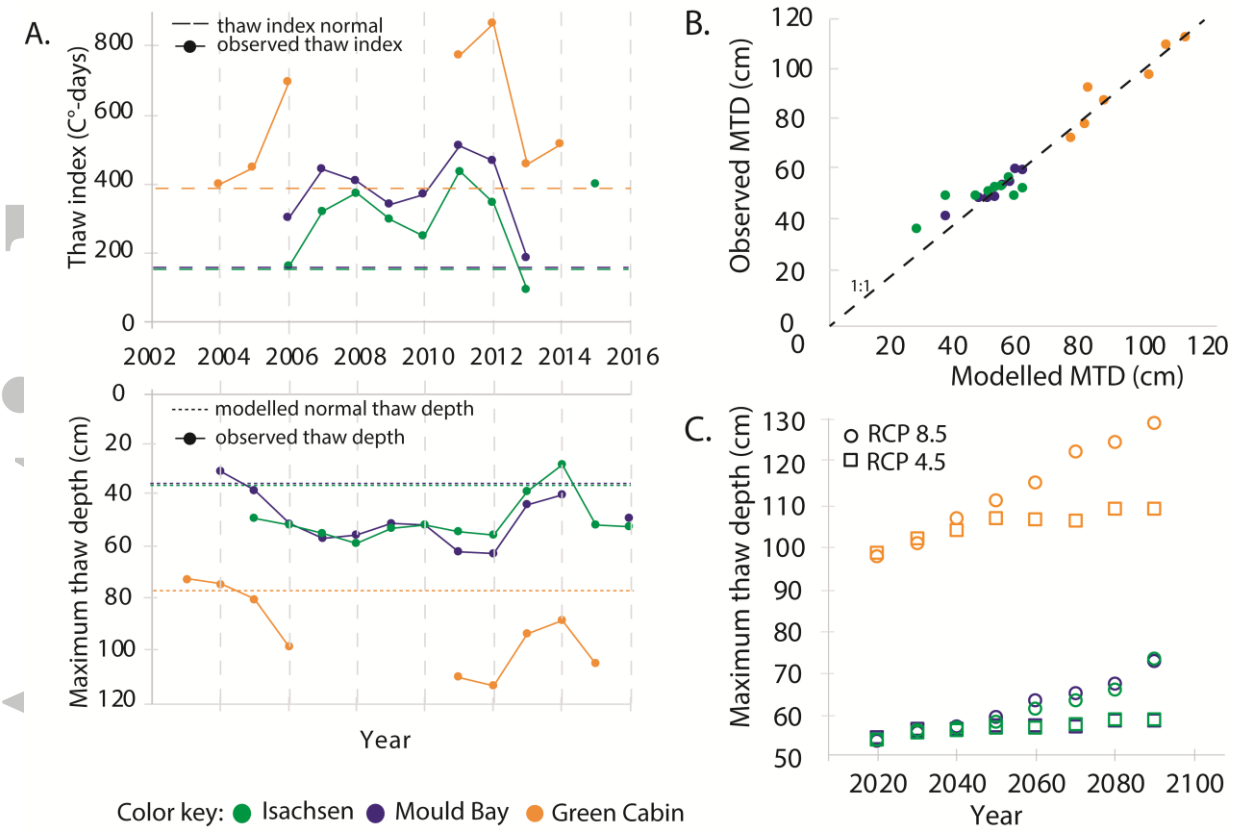

Figure 2. A. Top graph: TI (°C-days) through time for the three study sites. The dotted lines represent the thawing index normals (1979 to 2000, http://climate.weather.gc.ca/historical_data, Everett, 1968) for each site. Time on the *x*-axes is in calendar years. Bottom graph: Maximum thaw depth (cm) for each year at the three study sites. The dotted lines represent modelled historic maximum thaw depths calculated using the Stefan equation (eq. 1) and values derived from the TI normals shown in the top graph. B. Comparison of observed maximum thaw depths and thaw depths modelled using the Stefan equation and A values (eq. 2) derived from observed maximum thaw depths. C. Projected thaw depths for our three study sites under RCP 4.5 and 8.5. For all diagrams the symbology is as follows: Isachsen, green; Mould Bay, blue; Green Cabin, orange.

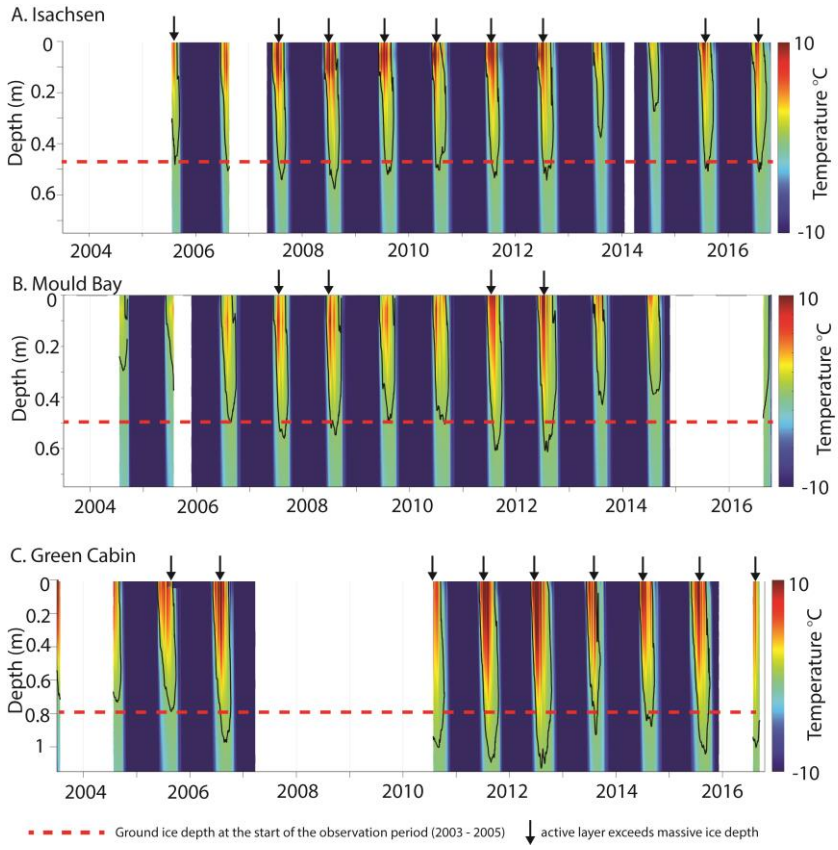

Figure 3. Thaw depth and temperature diagrams for: A. Isachsen, B. Mould Bay, and C. Green Cabin. Red dotted line shows ground ice depth at the start of the observation period. Black arrows indicate years where maximum thaw depth exceeds ground ice depth. The black continuous line is the 0°C isotherm in the ground.

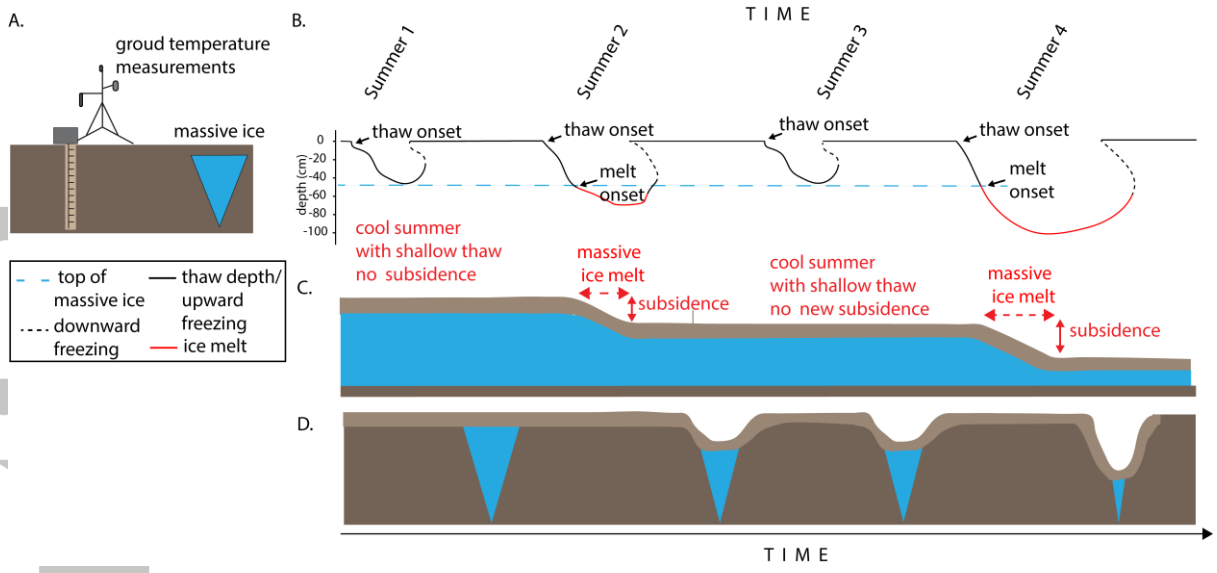

Figure 4. A schematic diagram of how summer thaw leads to rapid ice-wedge degradation. A. An illustration of our monitoring station set-up and source of ground temperature data in relation to near-surface massive ice. B. A conceptual diagram illustrating thaw front dynamics based on measurements taken at our study sites. C. A cross section of massive ice melt through time showing how protective sediment thickness remains the same despite active layer deepening, leading to cumulative melt throughout the thaw season. D. A cross section of ice wedge thaw through three summers where the depth of thaw exceeded the sediment overburden above ice-wedge ice, and one cool summer where no additional subsidence occurs.